Received 25 November 2009
Revised 3 June 2010,
26 July 2010
Accepted 28 July 2010

Prediction of a temperature-dependent electroosmotically driven microchannel flow with the Joule heating effect

Tony W.H. Sheu, S.H. Kuo and R.K. Lin
Department of Engineering Science and Ocean Engineering, National Taiwan University, Taipei, Taiwan

Abstract

Purpose – A convection-diffusion-reaction scheme is proposed in this study to simulate the high gradient electroosmotic flow behavior in microchannels. The equations governing the total electric field include the Laplace equation for the effective electrical potential and the Poisson-Boltzmann equation for the electrical potential in the electric double layer.

Design/methodology/approach – Mixed electroosmotic/pressure-driven flow in a straight microchannel is studied with the emphasis on the Joule heat in the equations of motion. The nonlinear behaviors resulting from the hydrodynamic, thermal and electrical three-field coupling and the temperature-dependent fluid viscosity, thermal conductivity, electrical permittivity, and conductivity of the investigated buffer solution are analyzed.

Findings – The solutions computed from the employed flux discretization scheme for the hydrodynamic, thermal and electric field equations have been verified to have good agreement with the analytical solution. Parametric studies have been carried out by varying the electrical conductivity at the fixed zeta potential and varying the zeta potential at the fixed electrical conductivity.

Originality/value – Investigation is also addressed on the predicted velocity boundary layer and the electric double layer near the negatively charged channel wall.

Keywords Convection-diffusion-reaction, Convection, Diffusion, Electroosmotic flow, Poisson-Boltzmann equation, Joule heating, Electric double layer, Forecasting

Paper type Research paper

Nomenclature

Greek symbols

c_i	= concentration
D_i	= diffusion coefficient of the ith species, m^2/s
D	= dielectric constant
e	= elementary charge, C
$\mathbf{E}$	= strength of the applied electric field
$\mathbf{f}, f$	= source term
h	= channel height
$\mathbf{I}$	= electrical current density, $C/s \cdot m^2$
k_1	= coefficient of the diffusion term
k_b	= Boltzmann constant, J/K

The financial support provided by the National Science Council under the grants NSC97-2221-E-002-250-MY3 and CQSE 97R0066-69 is gratefully acknowledged. Partial support from National Center for Theoretical Sciences (NCTS) and the computational hardware support from National Center of High-performance Computing (NCHC) and Computer Center of National Taiwan University are highly appreciated.

International Journal of Numerical Methods for Heat & Fluid Flow
Vol. 22 No. 5, 2012
pp. 554-575

0961-5539
DOI 10.1108/09615531211231244

n = buffer ion density, mol/m^3
n_0 = ion density bulk solution, mol/m^3
N_0 = Avagadro number ($N_0 = 6.02 \times 10^{23}$)
p = pressure
c_p = specific heat at constant pressure
q = Joule heat generation, W/m^3
Re = Reynolds number ($= U_{\text{ref}} h/\mu$)
T = absolute temperature, K
U_{ref} = reference velocity, m/s
$\mathbf{u}$ = velocity vector
u = velocity component along x direction
v = velocity component along y direction
z = valence of the ion
ξ = surface zeta potential, V
ν = Kinematic viscosity, m^2/s
Φ = $\equiv \phi + \psi$
ρ_e = space charge density
ε = permittivity of the buffer solution, C/mV
ϕ = externally applied electrical potential
ψ = electrical potential in EDL
ε_0 = permittivity of vacuum, C/mV
λ^* = Debye length, m
ρ = density of the investigated fluid, kg/m^3
κ = $\equiv h^2/\lambda^2$
$\lambda(T)$ = electrical conductivity of the buffer solution, s/m
λ_+ = equivalent ionic conductivity of the cations, m^{2}s/mol
λ_- = equivalent ionic conductivity of the anions, m^{2}s/mol
λ_{+0} = the value of λ_+ at room temperature, m^{2}s/mol
λ_{-0} = the value of λ_- at room temperature, m^{2}s/mol
η_+ = the number of moles of cation in the electrolyte, M
η_- = the number of moles of anion in the electrolyte, M
$\varepsilon(T)$ = dielectric constant of the electrolyte
$\mu(T)$ = viscosity of the electrolyte, Pa·s

1. Introduction

Due to the large surface-to-volume ratio in microchannels, liquid fluids in microchannels, subjected to an externally applied electrical field, can be affected by the formation of electric double layer (EDL). Near the charged surface, which is in contact with an electrolyte, EDL consists of a compact layer of immobile balanced charges and a diffuse layer of mobile ions. This counter ion shielding layer is normally characterized by the Debye length, which typically has a value of 10 nm or less. The interface between the compact (or Stern) layer and the diffuse layer, in which liquid velocity is equal to zero under the zero pressure gradient condition, is called the shear plane. In diffuse layer, counter ions in excess can cause the fluid to convect under the externally applied force. This electroosmotic phenomenon was observed by Reuss (1809). Such a bulk flow nature is now known as the direct consequence of electroosmosis since moving ions can make their surrounding fluids to flow by virtue of the fluid viscosity. The microchannel flow in EDL, which differs very much from the conventional Navier-Stokes flow, warrants therefore a fundamental study.

Thanks to the emerging micro-electro-mechanical system techniques, electroosmotic flows have been found in many complex microfluidic networks for the purposes of loading, mixing, and flushing. Due to the emerging lab-on-a-chip microfluidic devices, numerous experimental and computational studies have been conducted in the past for increasing our understanding of the electroosmotic phenomena in microchannels. Most of the former investigations addressed the hydrodynamic behavior that is featured with the plug-flow velocity type. The Joule heating in electrohydrodynamic field cannot only cause the electrolyte temperature to increase but can also result in a larger temperature gradient, which may dramatically affect electroosmotic flow, transport of bio-sample and sample separation. In addition to the low column separation efficiency, reduction of resolution and loss of the injected

samples, instability of low-Reynolds-number electrokinetic flows with the high gradient of electrical conductivity may occur inside the microchannel, which is subjected to a strong electric field (Lin *et al.*, 2004; Storey, 2005).

With the advent of high-performance computing facility and better knowledge about EHD in the design of MTAS, numerical investigation of Joule heating effect on the electroosmotic flow and the study of electrophenetic transport of solutes in microfluidic channels have become one of the focal research attentions in the area of EOF (Tang *et al.*, 2003, 2004, 2006; Horiuchi and Dutta, 2004; Garai and Chakraborty, 2009; Singh *et al.*, 2008; Arnold *et al.*, 2008). To optimize the DNA hybridization performance in microchannel, within which fluid flow will be driven by electrokinetic and pressure forces, one can also simulate the EOF equations (Das and Chakraborty, 2007; Das *et al.*, 2006). As the first step to investigate the onset of instability due to the time-dependent electric and hydrodynamic properties, which cannot result in negligible gradients (temperature-dependent electrical conductivity, for example) in solutes, electrohydrodynamics will be studied in the microchannel by taking the Joule heat into account in the formulation of energy equation. This work is therefore aimed to elucidate some insights of the formation of EDL and to enlighten its relation to the developed velocity boundary layer. The competition among the viscous force, pressure gradient force, and electrokinetic body force due to the EDL formed immediately adjacent to the bounding wall will be explored numerically.

The rest of this paper is organized as follows. In Section 2, the coupling equations for the hydrodynamic, electrical and thermal field variables are described at length. Joule heating will be taken into account in the energy equation. In addition to the inertia, viscous, and pressure gradient forces in the hydrodynamic system, the electrokinetic body force is also considered in the equations of motion for the calculation of solute acceleration and, then, the velocity in the resulting electrohydrodynamic system. The locally analytic convection-diffusion-reaction (CDR) scheme applied to approximate the spatial derivative terms shown in the system of six coupled equations will be described in Section 3 and is then verified in Section 4. The predicted results for the problems investigated at different conductivities and wall zeta potentials will then be discussed in Section 5. Finally, some conclusions drawn from this study will be summarized in Section 6.

2. Working equations

We will investigate the electrokinetic fluid flow, subjected to a wall zeta potential, at different electric conductivities in a straight microchannel to address the Joule heating effect on the electroosmotic flow velocity. A full coupling of the equations among the electric, hydrodynamic and thermal fields will be considered. For an incompressible electrolyte flow, subjected to an externally applied electric field, the continuity equation and Navier-Stokes equations can be expressed in terms of the electrolyte density (ρ), hydrodynamic pressure (p) and velocity ($\mathbf{u}$) given below:

$$\nabla \cdot \mathbf{u} = 0 \tag{1}$$

$$\frac{\partial \mathbf{u}}{\partial t} + (\mathbf{u} \cdot \nabla)\mathbf{u} = -\frac{1}{\rho}\nabla p + \nu \nabla^2 \mathbf{u} + \mathbf{f} \tag{2}$$

The source term $\mathbf{f}(\equiv \rho_e \mathbf{E})$ in equation (2) denotes the electrokinetic body force due to the formation of EDL along the no-slip bounding surface (Probstein, 1994), where ρ_e

is the local electric charge density. The strength of the applied electric field $\mathbf{E}$ can be normally expressed by the negative gradient of electrical potential Φ:

$$\mathbf{E} = -\nabla\Phi \tag{3}$$

At the steady state, Φ can be modelled by the following Poisson equation according to the theory of electrostatics:

$$\nabla^2(\varepsilon\Phi) = -\frac{\rho_e}{\varepsilon_0} \tag{4}$$

In the above, $\varepsilon_0 (= 8.854 \times 10^{-12}\,\mathrm{C/V \cdot m})$ and ε denote the permittivity of vacuum and fluid medium, respectively. Note that equation (4) is normally used to describe the ion and potential distributions in diffuse layer.

One can separate Φ into the electrical potential ϕ, which is developed due to the externally applied electric field, and the electrokinetic potential ψ. Based on this decomposition of solution variables, equation (4) can be rewritten as the sum of the following two equations (Masliyah, 1994):

$$\nabla \cdot \left(\lambda(T)\nabla\phi\right) = 0 \tag{5}$$

$$\nabla^2\left(\varepsilon(T)\psi\right) = -\frac{\rho_e}{\varepsilon_0} \tag{6}$$

In this study we assume that the electrical conductivity of the investigated electrolyte depends on the temperature as $\lambda(T) = \lambda_+(T)\eta_+ + \lambda_-(T)\eta_-$ S/m. Here, $\lambda_+(T)$ $(= \lambda_{+0} + 0.025\lambda_{+0}(T - 298.13)\,\mathrm{m^2S/mol})$ and $\lambda_-(T)$ $(= \lambda_{-0} + 0.025\lambda_{-0}$ $(T - 298.13)\,\mathrm{m^2S/mol})$ are denoted as the ionic conductivity of the cation and anion of the electrolyte, respectively (Weast *et al.*, 1986). As for η_+ and η_-, they represent the mole concentrations of cation and anion present in the electrolyte. Also, the fluid permittivity is assumed to vary exponentially with the absolute temperature T as $\varepsilon(T) = (305.7\exp(-T/219))/\varepsilon_{\mathrm{ref}}$ (Tang *et al.*, 2006). Since the electrolyte under current investigation is classified to be symmetric and univalent, ρ_e can be represented by the following expression (Probstein, 1994):

$$\rho_e = -\frac{2n_0ez}{\varepsilon_{\mathrm{ref}}}\sinh\left(\frac{ez\psi}{k_bT}\right) \tag{7}$$

In the above, $n_0 (= 6.02 \times 10^{20}\,1/\mathrm{m^3})$ is the density of positive or negative ion in the buffer, $e (= 1.6 \times 10^{-19}\,\mathrm{C})$ denotes the electron charge, and $z(\equiv 1)$ is the valence. In equation (7), k_b is known as the Boltzmann constant $(= 1.38 \times 10^{-23}\,\mathrm{J/K})$. Under the above conditions, equation (6) can be rewritten as follows for ψ (Hunter, 1981):

$$\nabla^2\left(\varepsilon\psi\right) = \frac{2n_0ez}{\varepsilon_0}\sinh\left(\frac{ez\psi}{k_bT}\right) \tag{8}$$

In the presence of an externally applied pair of electric field $(-\partial\phi/\partial x,\ -\partial\phi/\partial y)$ and electrokinetic field $(-\partial\psi/\partial x,\ -\partial\psi/\partial y)$ in the diffuse layer, Navier-Stokes equations can be expressed as follows:

$$\rho\left(\frac{\partial u}{\partial t}+u\frac{\partial u}{\partial x}+v\frac{\partial u}{\partial y}\right)=-\frac{\partial p}{\partial x}+\frac{\partial}{\partial x}\left(\mu(T)\frac{\partial u}{\partial x}\right)+\frac{\partial}{\partial y}\left(\mu(T)\frac{\partial u}{\partial y}\right)-\rho_e\left(\frac{\partial \phi}{\partial x}+\frac{\partial \psi}{\partial x}\right) \tag{9}$$

$$\rho\left(\frac{\partial v}{\partial t}+u\frac{\partial v}{\partial x}+v\frac{\partial v}{\partial y}\right)=-\frac{\partial p}{\partial y}+\frac{\partial}{\partial x}\left(\mu(T)\frac{\partial v}{\partial x}\right)+\frac{\partial}{\partial y}\left(\mu(T)\frac{\partial v}{\partial y}\right)-\rho_e\left(\frac{\partial \phi}{\partial y}+\frac{\partial \psi}{\partial y}\right) \tag{10}$$

For modelling the Joule heating effect in EOF, one can adopt the consistent scaling introduced in Nithiarasu and Lewis (2008). In this study we normalize the dependent and independent variables in a different way given by $x^*=x/H$, $y^*=y/H$, $t^*=(U_{\text{ref}}t)/H$, $u^*=u/U_{\text{ref}}$, $v^*=v/U_{\text{ref}}$, $p^*=p/\rho U_{\text{ref}}^2$ $\mu^*=\mu(T)/\mu_{\text{ref}}$, $\psi^*=(ze\psi)/(k_bT)$, $n_+^*=n_+/n_0$, $n_-^*=n_-/n_0$, $U_{\text{ref}}=-(\varepsilon_{\text{ref}}\varepsilon_0\xi\Phi_{\text{ref}})/(\mu_{\text{ref}}L)$. The resulting dimensionless working equations, in addition to equation (1), are summarized as follows:

$$\frac{\partial}{\partial x}\left(\lambda(T)\frac{\partial \phi}{\partial x}\right)+\frac{\partial}{\partial y}\left(\lambda(T)\frac{\partial \phi}{\partial y}\right)=0 \tag{11}$$

$$\frac{\partial}{\partial x}\left(\varepsilon(T)\frac{\partial \psi}{\partial x}\right)+\frac{\partial}{\partial y}\left(\varepsilon(T)\frac{\partial \psi}{\partial y}\right)=\frac{2H^2z^2e^2n_0}{k_bT\varepsilon_{\text{ref}}\varepsilon_0}\sinh(\psi) \tag{12}$$

$$\frac{\partial u}{\partial t}+u\frac{\partial u}{\partial x}+v\frac{\partial u}{\partial y}=-\frac{\partial p}{\partial x}+\frac{1}{Re}\frac{\partial}{\partial x}\left(\mu(T)\frac{\partial u}{\partial x}\right)+\frac{1}{Re}\frac{\partial}{\partial y}\left(\mu(T)\frac{\partial u}{\partial y}\right)+\frac{2Hzen_0\sinh(\psi)}{\rho U_{\text{ref}}^2}\frac{\partial \phi}{\partial x}+\frac{2n_0k_bT\sinh(\psi)}{\rho U_{\text{ref}}^2}\frac{\partial \psi}{\partial x} \tag{13}$$

$$\frac{\partial v}{\partial t}+u\frac{\partial v}{\partial x}+v\frac{\partial v}{\partial y}=-\frac{\partial p}{\partial y}+\frac{1}{Re}\frac{\partial}{\partial x}\left(\mu(T)\frac{\partial v}{\partial x}\right)+\frac{1}{Re}\frac{\partial}{\partial y}\left(\mu(T)\frac{\partial v}{\partial y}\right)+\frac{2Hzen_0\sinh(\psi)}{\rho U_{\text{ref}}^2}\frac{\partial \phi}{\partial y}+\frac{2n_0k_bT\sinh(\psi)}{\rho U_{\text{ref}}^2}\frac{\partial \psi}{\partial y} \tag{14}$$

where Re is defined by $(\rho U_{\text{ref}}H)/\mu_{\text{ref}}$. Note that all superscripts "*" have been omitted for the sake of brevity. The electrolyte viscosity under current investigation is assumed to vary with the temperature according to $\mu(T)=2.761\times10^{-6}\exp(1713/T)\,Pa\cdot s/\mu_{\text{ref}}$ (Tang *et al.*, 2006).

In mixed formulation, the divergence-free constraint equation (1) will be solved together with the momentum equations (13) and (14). A direct employment of the incompressibility constraint equation will, however, increase both of the matrix condition number and matrix size. To overcome this computational difficulty, we adopt the segregated approach by reformulating the mass conservation equation in terms of the pressure variable by virtue of $(\partial/\partial x)(13)+(\partial/\partial y)(14)$ and, then, employing equation (1).

The resulting pressure Poisson equation, which is derived to replace the mass conservation equation (1), is as follows:

$$\nabla^2 p = \frac{\partial}{\partial x}\left[-\rho\left(\frac{\partial u}{\partial t}+u\frac{\partial u}{\partial x}+v\frac{\partial u}{\partial y}\right)+\frac{\partial}{\partial x}\left(\mu(T)\frac{\partial u}{\partial x}\right)+\frac{\partial}{\partial y}\left(\mu(T)\frac{\partial u}{\partial y}\right)-\rho_e\left(\frac{\partial \phi}{\partial x}+\frac{\partial \psi}{\partial x}\right)\right] + \frac{\partial}{\partial y}\left[-\rho\left(\frac{\partial v}{\partial t}+u\frac{\partial v}{\partial x}+v\frac{\partial v}{\partial y}\right)+\frac{\partial}{\partial x}\left(\mu(T)\frac{\partial v}{\partial x}\right)+\frac{\partial}{\partial y}\left(\mu(T)\frac{\partial v}{\partial y}\right)-\rho_e\left(\frac{\partial \phi}{\partial y}+\frac{\partial \psi}{\partial y}\right)\right] \tag{15}$$

Since the permittivity (ε) and electrical conductivity (λ) in the buffer solution are both dependent on the temperature, energy equation for modeling the time-evolving temperature needs to be derived. By taking into account the Joule heat for obtaining an accurate temperature distribution in the electroosmotic flowfield, the governing equation, cast in its dimensional form, for the conservation of thermal energy is given below according to the first-law of thermodynamics:

$$\rho c_p\left(u\frac{\partial T}{\partial x}+v\frac{\partial T}{\partial x}\right)=\frac{\partial}{\partial x}\left(k_1(T)\frac{\partial T}{\partial x}\right)+\frac{\partial}{\partial y}\left(k_1(T)\frac{\partial T}{\partial y}\right)+q \tag{16}$$

In the above, c_p is the specific heat capacity, k_1 the thermal conductivity and q the Joule heat. Note that heat generation due to the viscous dissipation is normally quite small and can be neglected. According to Ohm's law, generation of energy due to Joule heating can be expressed as $q = (\mathbf{I}\cdot\mathbf{I})/\lambda(T)$ (Tang *et al.*, 2003), where $\mathbf{I}$ denotes the electrical current density in the solution. In the current study, the electrical current density is resulted from $\mathbf{E}\lambda$, which is due to the electric field applied to the conductive solution. As for $\rho_e\mathbf{u}$, it results from the net charged density moving along with the fluid flow. In other words, the electrical current density $\mathbf{I}$ can be expressed as:

$$\mathbf{I} = \rho_e\mathbf{u} + \lambda(T)\mathbf{E} \tag{17}$$

Substituting equation (17) for $\mathbf{I}$ into Ohm's law and, then, into equation (16), the energy equation for T can be derived as follows:

$$\rho c_p\left(\frac{\partial T}{\partial t}+u\frac{\partial T}{\partial x}+v\frac{\partial T}{\partial y}\right)=\frac{\partial}{\partial x}\left(k_1(T)\frac{\partial T}{\partial x}\right)+\frac{\partial}{\partial y}\left(k_1(T)\frac{\partial T}{\partial y}\right)+\frac{(u\rho_e+E_x\lambda(T))^2+(v\rho_e+E_y\lambda(T))^2}{\lambda(T)} \tag{18}$$

Based on the chosen normalization quantities given by $T^* = (T - T_{\text{ref}})/(T_0 - T_{\text{ref}})$, $k^* = k_1(T)/k_{\text{ref}}$, $n_+^* = n_+/n_0$, $n_-^* = n_-/n_0$, the dimensionless energy equation containing the Joule heat is derived as follows:

$$\frac{\partial T}{\partial t}+u\frac{\partial T}{\partial x}+v\frac{\partial T}{\partial y}=\frac{1}{Pr\,Re}\left[\frac{\partial}{\partial x}\left(k_1(T)\frac{\partial T}{\partial x}\right)+\frac{\partial}{\partial y}\left(k_1(T)\frac{\partial T}{\partial y}\right)\right]+\frac{H(u\rho_e+E_x\lambda(T))^2+H(v\rho_e+E_y\lambda(T))^2}{\rho c_p U_{\text{ref}}(T_0-T_{\text{ref}})\lambda(T)} \tag{19}$$

It is worthy to note that the conservation equations for incompressible electrolyte solution, ionized fluid flow with the electroosmotic body force, the Laplace equation for the external electric field, the Poisson-Boltzmann equation for the zeta potential, and the conservation of energy with Joule heat can be cast into the following generalized form:

$$\bar{\phi}_t + u\bar{\phi}_x + v\bar{\phi}_y = \Gamma\nabla^2\bar{\phi} + f \tag{20}$$

The definitions of all field variables $\bar{\phi}$, diffusivities Γ, and f are tabulated in Table I.

3. Numerical model

Unlike the Newtonian fluid flow, velocity gradient of EOF in the microchannel can be very large near the bounding wall. To sharply resolve this high-gradient velocity, we present below the computationally very accurate and stable CDR scheme.

The model equation suitable to represent each equation in the electrohydrodynamic system can be generally expressed as follows:

$$\bar{\phi}_t + u\bar{\phi}_x + v\bar{\phi}_y - k\nabla^2\bar{\phi} + c\bar{\phi} = f \tag{21}$$

For simplicity, calculation of the above CDR differential equation is subjected to a specified boundary value of $\bar{\phi}$. In the above, k and c denote the diffusion coefficient and the reaction coefficient, respectively. In what follows, the values of u, v, k and c will be assumed to be uniform. By applying the operator splitting method of Peaceman and Rachford (1955), the solution for equation (21) can be step-by-step calculated from the two equations given below:

$$u\bar{\phi}^*_x - k\bar{\phi}^*_{xx} + c\bar{\phi}^* = f_1 \tag{22}$$

$$v\bar{\phi}^{n+1}_y - k\bar{\phi}^{n+1}_{yy} + c\bar{\phi}^{n+1} = f_2 \tag{23}$$

In the above, $f_1 = f^* - v\bar{\phi}^n_y + k\bar{\phi}^n_{yy}$ and $f_2 = f^{n+1} - u\bar{\phi}^*_x + k\bar{\phi}^*_{xx}$.

Thanks to the above two equations, we are led to know that the key to accurately solve equation (21) depends on the chosen discretization scheme for the following model equation:

$$u\bar{\phi}_x - k\bar{\phi}_{xx} + c\bar{\phi} = \bar{f} \tag{24}$$

Our strategy of approximating equation (24) is to employ its general solution given below:

$$\bar{\phi}(x) = c_1 e^{\lambda_1 x} + c_2 e^{\lambda_2 x} + \frac{\bar{f}}{c} \tag{25}$$

where $\lambda_{1,2} = (u \pm \sqrt{u^2 + 4ck})/2k$ and c_1 and c_2 are two arbitrary constants. By applying the artificial viscosity model, the discrete equation for equation (24) at an interior node i is expressed as:

$$\left(-\frac{u}{2h} - \frac{m}{h^2} + \frac{c}{6}\right)\bar{\phi}_{i-1} + 2\left(\frac{m}{h^2} + \frac{c}{3}\right)\bar{\phi}_i + \left(\frac{u}{2h} - \frac{m}{h^2} + \frac{c}{6}\right)\bar{\phi}_{i+1} = \bar{f} \tag{26}$$

where h is the mesh size. The exact solutions given by $\bar{\phi}_{i+1} = c_1 e^{\lambda_1 h} e^{\lambda_1 x_i} + c_2 e^{\lambda_2 h} e^{\lambda_2 x_i} + (\bar{f}/c)$, $\bar{\phi}_i = c_1 e^{\lambda_1 x_i} + c_2 e^{\lambda_2 x_i} + (\bar{f}/c)$ and $\bar{\phi}_{i-1} = c_1 e^{-\lambda_1 h} e^{\lambda_1 x_i} + c_2 e^{-\lambda_2 h} e^{\lambda_2 x_i} + (\bar{f}/c)$ are

Continuity equation		*Energy equation*	*x-momentum equation*
$\bar{\phi}$	p	T	u
Γ	1	$\frac{k_f}{Pr \cdot Re}$	$\frac{\mu}{Re}$
f	$-\left(\frac{\partial u}{\partial x}\right)^2 - \left(\frac{\partial v}{\partial y}\right)^2 - 2\frac{\partial u}{\partial x}\frac{\partial v}{\partial y} + \frac{1}{Re}\left[\frac{\partial \mu}{\partial x}\left(\frac{\partial^2 u}{\partial x^2} + \frac{\partial^2 u}{\partial y^2}\right) + \frac{\partial \mu}{\partial y}\left(\frac{\partial^2 v}{\partial x^2} + \frac{\partial^2 v}{\partial y^2}\right)\right]$	$\frac{H(\alpha\rho_e + E_x\lambda(T))^2 + H(\alpha\rho_e + E_y\lambda(T))^2}{\rho c_p U_{\text{ref}}(T_0 - T_{\text{ref}})\lambda(T)}$	$+\frac{2Hze n_0 \sinh(\psi)}{\rho U_{\text{ref}}^2}\frac{\partial \phi}{\partial x} + \frac{2n_0 k_b T \sinh(\psi)}{\rho U_{\text{ref}}^2}\frac{\partial \psi}{\partial x}$
	$+\frac{\partial}{\partial x}\left(\frac{2Hze n_0 \sinh(\psi)}{\rho U_{\text{ref}}^2}\frac{\partial \phi}{\partial x} + \frac{2n_0 k_b T \sinh(\psi)}{\rho U_{\text{ref}}^2}\frac{\partial \psi}{\partial x}\right)$		
	$+\frac{\partial}{\partial y}\left(\frac{2Hze n_0 \sinh(\psi)}{\rho U_{\text{ref}}^2}\frac{\partial \phi}{\partial y} + \frac{2n_0 k_b T \sinh(\psi)}{\rho U_{\text{ref}}^2}\frac{\partial \psi}{\partial y}\right)$		
y-momentum equation		*Electric equation*	*Zeta potential*
$\bar{\phi}$	v	ϕ	ψ
Γ	$\frac{\mu}{Re}$	λ	ε
f	$-\frac{2Hze n_0 \sinh(\psi)}{\rho U_{\text{ref}}^2} E_y + \frac{2n_0 k_b T \sinh(\psi)}{\rho U_{\text{ref}}^2}\psi_y$	0	$\frac{2H^2 z^2 e^2 n_0}{k_b T \varepsilon_{\text{ref}} \varepsilon_0} \sinh(\psi)$

Table I.
Summary of the transport equations shown in equation (20)

then substituted into equation (26) to get the following close-form expression for the coefficient m shown in equation (26) (Sheu *et al.*, 2000):

$$m = h^2\left\{\frac{c/3 + c/6\cosh(\bar{\lambda}_1)\cosh(\bar{\lambda}_2) + u/2h\ \sinh(\bar{\lambda}_1)\cosh(\bar{\lambda}_2)}{\cosh(\bar{\lambda}_1)\cosh(\bar{\lambda}_2) - 1}\right\} \tag{27}$$

where:

$$(\bar{\lambda}_1, \bar{\lambda}_2) = \left(\frac{uh}{2k}, \sqrt{\left(\frac{uh}{2k}\right)^2 + \frac{ch^2}{k}}\right).$$

Approximation of $\partial p/\partial x$ or $\partial p/\partial y$ term in non-staggered grids can normally result in spurious even-odd oscillations (Patankar, 1980). It is therefore essential to suppress these erroneous checkerboarding pressure solutions when solving the incompressible viscous equations in collocated grids. In this study, $M_j(\equiv h\bar{\phi}_x)$ and $N_j(\equiv h^2\bar{\phi}_{xx})$ will be implicitly calculated from the following two implicit equations to eliminate the even-odd decoupling problem (Sheu and Lin, 2003):

$$\begin{aligned}\alpha_0 M_{j+1} + \beta_0 M_j + \gamma_0 M_{j-1} &= a_0(\bar{\phi}_{j+2} - \bar{\phi}_{j+1}) + b_0(\bar{\phi}_{j+1} - \bar{\phi}_j) \\ &+ c_0(\bar{\phi}_j - \bar{\phi}_{j-1}) + d_0(\bar{\phi}_{j-1} - \bar{\phi}_{j-2})\end{aligned} \tag{28}$$

and:

$$\alpha_1 N_{j+1} + \beta_1 N_j + \gamma_1 N_{j-1} = a_1\bar{\phi}_{j+2} + b_1\bar{\phi}_{j+1} + c_1\bar{\phi}_j + d_1\bar{\phi}_{j-1} + e_1\bar{\phi}_{j-2} \tag{29}$$

Provided that $(\alpha_0, \beta_0, \gamma_0, a_0, b_0, c_0, d_0, e_0) = (1/5, 3/5, 1/5, 1/60, 29/60, 29/60, 1/60)$ and $(\alpha_1, \beta_1, \gamma_1, a_1, b_1, c_1, d_1, e_1) = (1, 11/2, 1, 3/8, 6, -51/4, 6, 3/8)$, the approximated equations for $\bar{\phi}_x$ and $\bar{\phi}_{xx}$ can be shown to have the sixth-order accuracy.

The implicit equations for M and N at the nodes located immediately adjacent to the boundary points can be derived by specifying $d_0 = e_1 = 0$ and $a_0 = a_1 = 0$ at the nodes next to the left and the right boundaries, respectively. The values of $(\alpha_0, \beta_0, \gamma_0, a_0, b_0, c_0, d_0, e_0) = (3/10, 3/5, 1/10, 1/30, 19/30, 1/3, 0)$ and $(1/10, 3/5, 3/10, 0, 1/3, 19/30, 1/30)$ can be analytically derived for the nodal points located next to the left and the right boundaries, respectively, by expanding the terms shown in equation (28) in Taylor series. Similarly, the coefficients shown in equation (29) for N_j can be exactly derived as $(\alpha_1, \beta_1, \gamma_1, a_1, b_1, c_1, d_1, e_1) = (1, 10, 1, 0, 12, -24, 12, 0)$.

For effectively solving the incompressible momentum equations, which are coupled with the transport equations for the energy, electric field and electrokinetic potential, we apply in this study the regularized solution algorithm proposed previously in Sheu and Chiu (2007). The idea of developing this iterative algorithm is to replace the incompressible constraint equation with the differential equation derived from equation (15). One can refer to Sheu and Chiu (2007), which detailed the currently applied Divergence Free Compensated solution algorithm, for additional details.

4. Verification study

There are very few analytic solutions available in the literature for the microchannel flow equations, subject to a combined action of electroosmotic force and an imposed

pressure gradient, for us to validate the code. In addition to the analytic problem given in Chakraborty (2006), we will choose in this study the electroosmotic/pressure driven problem of Dutta and Breskok (2001) to validate the employed scheme. Since the channel height (h) is much shorter than the channel length, the resulting steady-state channel flow is assumed to be fully developed. Given these assumptions, the dimensionless streamwise momentum equation, subject to the dimensionless electroosmotic potential ψ, can be simplified as Dutta and Breskok (2001):

$$\frac{\partial p^*}{\partial \xi} = \frac{\partial^2 U}{\partial \eta^2} + \frac{\partial^2 \psi^*}{\partial \eta^2} \tag{30}$$

where $U = u/U_{ref}$, $p^* = (ph)/(\mu U_{ref})$, $\xi = x/h$ and $\eta = y/h$. Note that ψ^* is governed by $(d^2\psi^*)/(d\eta^2) = \beta sinh\,(\alpha\psi^*)$, where α is the ionic energy parameter and $\beta(\equiv (wh)^2/\alpha)$ has association with the Debye-Hückel parameter $w(=1/\lambda^*)$ or the Debye length λ^*. The electroosmotic potential has been analytically derived to have the expression as follows in Hunter (1981):

$$\psi^* = \frac{4}{\alpha}\tanh^{-1}\left[\tanh\left(\frac{\alpha}{4}\right)\exp\left(-\sqrt{\alpha\beta}\eta^*\right)\right] \tag{31}$$

Note that $\eta^*(\equiv 1 - |\eta|)$ denotes the normalized distance measured from the wall. It can be observed from Figure 1 that the predicted zeta potential agrees well with the exact solution (31).

Under the non-zero pressure gradient condition, one can integrate equation (30) to get the following dimensionless velocity profile in the mixed electroosmotic/pressure gradient flow (Dutta and Breskok, 2001):

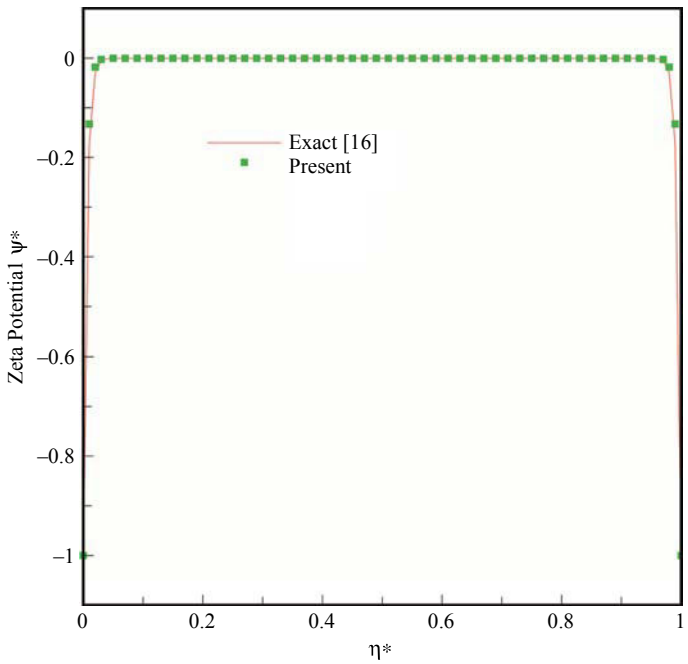

Figure 1.
Comparison of the predicted and exact zeta potentials which are plotted against η^*

$$U(\eta) = -\frac{1}{2}\frac{dp^*}{d\xi}\left(1-\eta^2\right) + \left[1-\psi^*(\eta)\right] \tag{32}$$

Provided that the zero pressure gradient condition is considered, equation (31) has been studied previously by Burgreen and Nakache (1964). Note that the case investigated at $dp^*/d\xi = 0$ corresponds to the pure plug-like flow, which has been experimentally observed in Dutta and Breskok (2001). Analysis will be carried out at $\alpha = 1$ and $\beta = 10^4$ for the cases with two favorable pressure gradients $\chi (\equiv dp^*/d\xi = -0.5$ and $-1.0)$, two adverse pressure gradients ($= dp^*/d\xi = 0.5$ and 1.0) and zero pressure gradient. One can clearly see from Figure 2 that the computed velocity distributions in the mixed electroosmotic/pressure driven flow field compare favorably with the analytic solutions, given by equation (32), computed at the five chosen values of $dp^*/d\xi$.

5. Discussion of results

The electroosmotic fluid flow under current investigation is bounded by two parallel silica walls, which are both immersed in an aqueous solution and are negatively charged by way of hydration. The resulting charged surfaces can attract positive ions (or counter ions) moving towards the wall and form, therefore, a Stern layer (or compact layer), which shields the surface charges. The negative charges in the solution will, on the other hand, be repelled from the solid walls. Because of the thermal motion, ions of

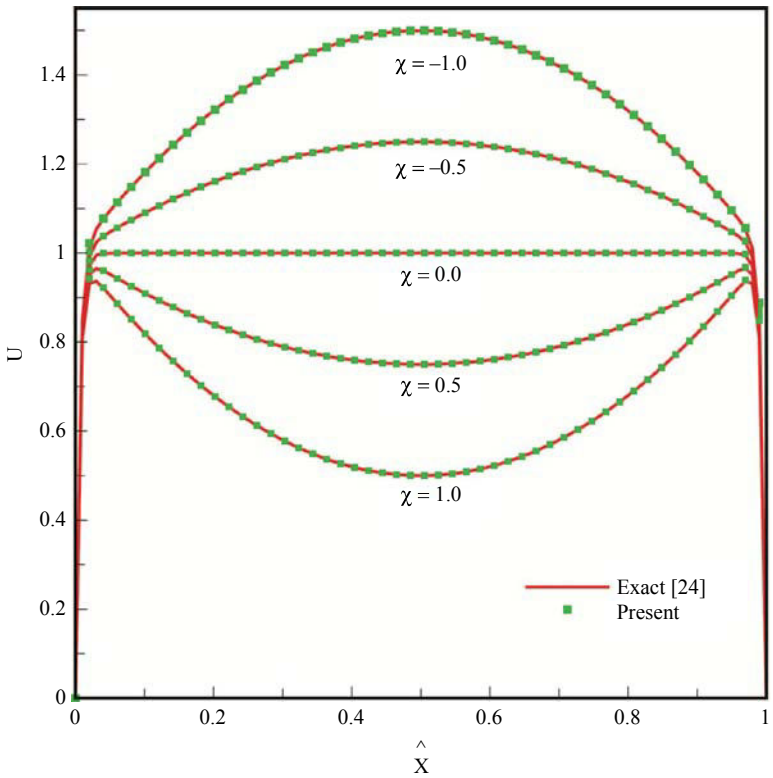

Figure 2.
Comparison of the predicted and exact velocity profiles for the cases investigated at different pressure gradients χ

opposite-sign are not bound to the wall surface but will rather be dispersed in the vicinity of wall surface. Such a charge separation is the outcome of electrostatic force and thermal motion in the respective Stern layer and diffuse layer (or Gouy-Chapman layer). Due to the formation of an EDL, the spatially varying electrical potential within the channel is changed from zero at a location far from the wall and reaches the maximum magnitude in regions near the wall. An electric field will then be established in the vicinity of solid-liquid interface due to the attraction-and-repulsion of positive charges.

In this study, we intend to know how the applied electric field and the established electrical potential field in the solution due to attracting-and-repelling charges to/from the wall can affect the hydrodynamic behavior in the microchannel. The immobile positive ions are seen in the Stern layer and the mobile ions show their presence in the diffuse layer. We are also aimed to know the distance, measured from the wall, beyond which the surface charges can no longer affect the ion distribution in the solution. We will later on compare the predicted Debye length and $\lambda^* = ((8\pi m_0 e^2 z^2)/(Dk_b T))^{-1/2}$ (Dutta and Breskok, 2001), where n_0 is the ion density in the bulk solution, k_b the Boltzmann constant, and D the dielectric constant. The Debye length is set as 2.15×10^{-7} m for the ion concentration of *NaCl* at room temperature 298°K.

In the straight channel of width 1×10^{-4} m and length 5×10^{-4} m schematic in Figure 3, the electric potential with an unit voltage is applied at the left entrance and the right exit is grounded. With this externally applied electric field, the positive ions within the EDL tend to move towards the cathode end. The ions moving along the streamwise direction can, in turn, cause the electrically driven flow motion to occur in the channel due to fluid viscosity.

The working medium we consider in this case is *NaCl*, which has the following properties, namely, the concentration (10^{-4} M), density (1,000 kg/m^3), dielectric constant (78.4) and specific heat (4,180 J/kg·K). The governing equations derived in Section 2 will be solved subject to the following prescribed boundary conditions at the channel inlet, channel outlet, and the no-slip walls, respectively.

Inlet:

$$T = 0, \quad \phi = 1, \quad \frac{\partial \psi}{\partial x} = 0, \quad \frac{\partial u}{\partial x} = \frac{\partial v}{\partial x} = 0, \quad \frac{\partial p}{\partial x}$$

$$= -\frac{\partial u}{\partial t} - v \frac{\partial u}{\partial y} \frac{1}{Re} \left(\frac{\partial \mu}{\partial y} \frac{\partial u}{\partial y} + \mu \frac{\partial^2 u}{\partial y^2} \right) + f_1 \tag{33}$$

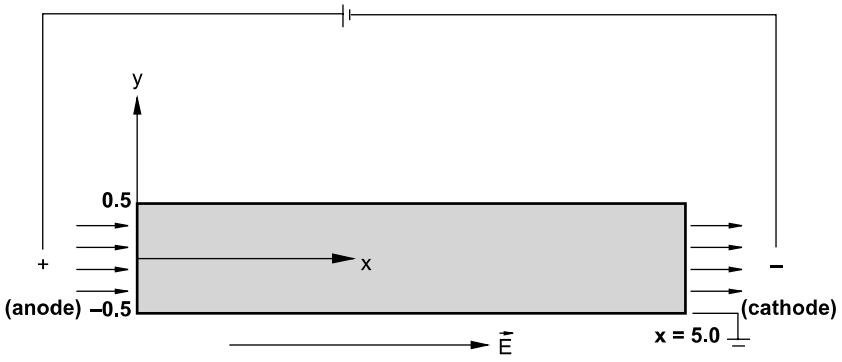

Figure 3.
Schematic of the investigated microchannel

Outlet:

$$\frac{\partial T}{\partial x} = 0, \quad \phi = 0, \quad \frac{\partial \psi}{\partial x} = 0, \quad \frac{\partial u}{\partial x} = \frac{\partial v}{\partial x} = 0, \quad p = 0 \tag{34}$$

Wall:

$$\psi = \xi_0, \quad u = v = 0, \quad \frac{\partial \phi}{\partial y} = 0, \quad \frac{\partial p}{\partial y} = 0, \quad \frac{\partial T}{\partial y} = 0 \tag{35}$$

Calculation will be carried out at $Re = 0.23$, Pr (Prandtl number $\equiv (\mu_{ref}\ c_p)/k_{ref} = 5.9$) and Sc (Schmidt number $\mu_{ref}/(\rho_f D) = 42611$) in the uniform mesh with 1001 and 101 nodal points distributed along the x and y directions, respectively. Four different electrical conductivities, namely, $\lambda_1 = 1.264 \times 10^{-6}$ (obtained at room temperature), $\lambda_2 = 10\lambda_1$, $\lambda_3 = 50\lambda_1$ and $\lambda_4 = 100\lambda_1$ will be investigated with the two zeta potentials fixed at $\psi = -1$ and 1.94.

Figure 4 shows the predicted temperature profiles for $T(x, 0)$ along the centerline. It can be clearly observed from this figure that the predicted temperatures for each investigated λ value keep increasing along the streamwise direction with their peak values found at the locations that are slightly downstream of the channel inlet. After reaching the peak temperature, T begins to change very slowly and it will monotonically approach to a nearly constant value. The Joule heats generated in the fluids are plotted in Figure 5 at the four investigated conductivities. The predicted Joule heats at the higher values of λ are seen to decrease quickly from the channel inlet and become gradually uniform. The higher the electrical conductivity, the larger amount of Joule heat can be generated. This explains why the predicted temperature shown in Figure 4 is found to increase its value with the electrical conductivities owing to the generation of a larger Joule heat.

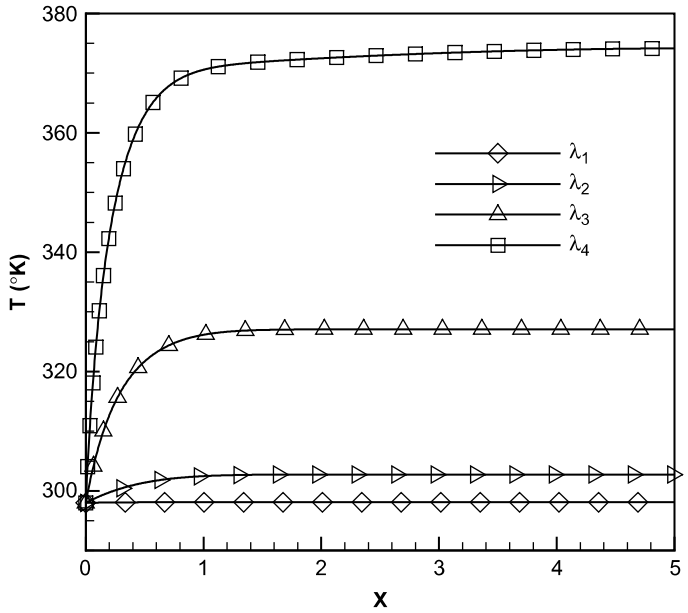

Figure 4.
Comparison of the predicted temperature profiles T at $y = 0$ (plane of symmetry) against the streamwise coordinate x for the four investigated electrical conductivities, namely, $\lambda_4 = 100\lambda_1$, $\lambda_3 = 50\lambda_1$, $\lambda_2 = 10\lambda_1$ and λ_1

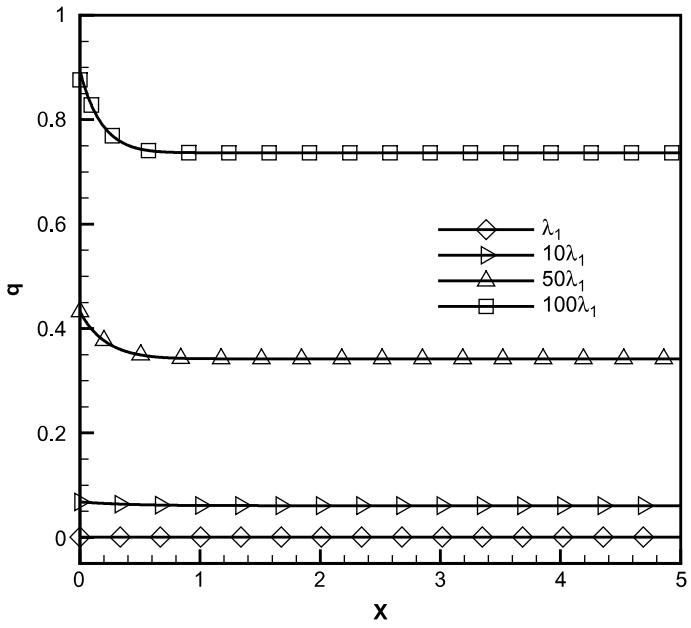

Figure 5.
The plot of the computed Joule heats against x at the four investigated electrical conductivities

The velocity profiles u (x, y) plotted at $x = 0$, 1, 2.5, 4, 5 in Figure 6 confirm that the predicted velocity conserves the mass very well in the current electroosmotic flow simulation. It is interesting to find from these predicted u-profiles that the velocity magnitude has a much sharper change than that found in the pressure-driven laminar flow velocity near the no-slip wall. In an attempt to elucidate the mechanism that causes such a sharp boundary layer, which manifests the electroosmotic flow, we plot the computed values of $-\rho_e(\partial\phi/\partial x)$, $-\rho_e(\partial\phi/\partial y)$, $-\rho_e(\partial\psi/\partial x)$, and $-\rho_e(\partial\psi/\partial y)$ against y in Figure 7 at $x = 2.5$. It can be seen that the y-component forces are smaller than the x-component forces. In x-momentum equation (9), the value of $-\rho_e(\partial\phi/\partial x)$ is greater than $-\rho_e(\partial\psi/\partial x)$ mainly because of $\sinh(\psi)$, which varies dramatically in the vicinity of $y = 0.5$ (no-slip wall) and its value becomes nominally unchanged with respect to y in most of the channel. This explains why EOF exhibits a much sharper streamwise velocity gradient near the wall than that predicted in the pressure-driven flow that is investigated at a fairly small Reynolds number.

Discussion of the results is followed by investigating the effect of non-uniform material properties, which are assumed to be varied with the temperature according to $\varepsilon(T) = 305.7\exp(1713/T)$, $\lambda_{\pm}(T) = \lambda_{0\pm} + 0.025\lambda_{\pm}(T - 298)$, $\mu(T) = 2.761 \times 10^{-6}T$, and $k_1(T) = 0.6 + 2.5 \times 10^{-5}T$, on the streamwise velocity profile $u(x, y)$. For this reason, we plot u $(x = 2.5, y)$ in Figure 8 for the case investigated at $\psi = -1$ and $\lambda = \lambda_1$ and then compare this velocity with that investigated at room temperature $T = 298$°K. Since temperature can affect the physical properties λ, ε, μ and k_1, we find out from the predicted results that both k_1 and λ have comparatively uniform contours than those of ε and μ.

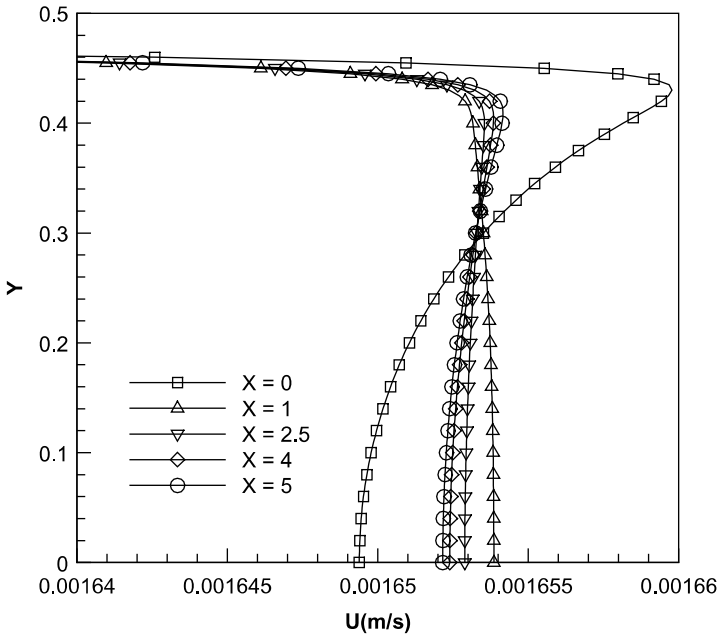

Figure 6.
The predicted velocity profiles u (x, y) at the five chosen streamwise locations for the case investigated at λ_1 and $\psi = -1$

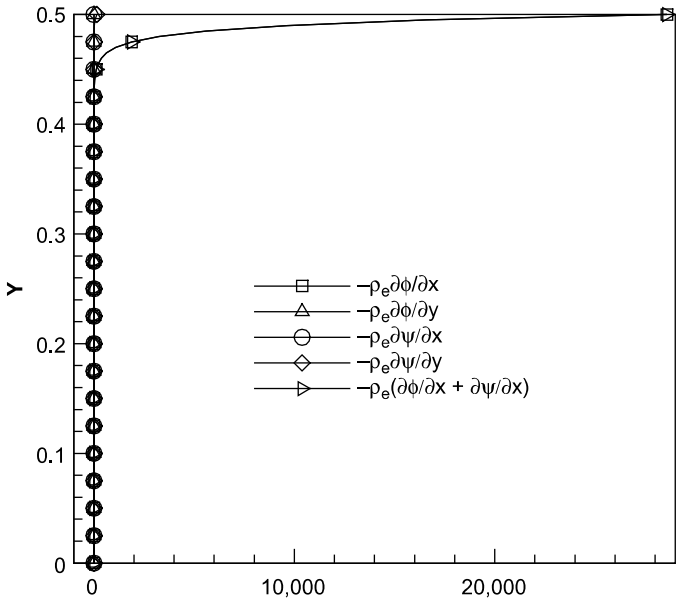

Figure 7.
The predicted values of $-\rho_e(\partial\phi/\partial x)$, $-\rho_e(\partial\phi/\partial y)$, $-\rho_e(\partial\psi/\partial x)$ and $-\rho_e(\partial\psi/\partial y)$, which are plotted against the transverse coordinate y at $x = 2.5$, for the case investigated at $\psi = -1$ and $\lambda = \lambda_1$

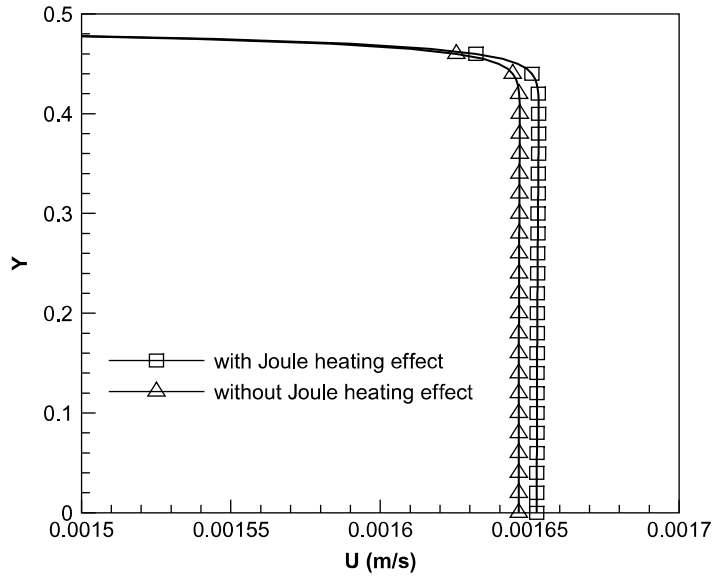

Figure 8.
Comparison of the predicted velocity profiles u ($x = 0.5$, y) for the cases with/without consideration of Joule heat

We then investigated the cases at the fixed electrical conductivity λ_1 and at the four zeta potentials $\psi(= -1, -1.5, -1.94$ and $-2.5)$. First, to examine the effect of the applied zeta potential on the velocity, we plot in Figure 9 the velocity profiles against y at $x = 2.5$ for the cases investigated at $\psi = -1, -1.5, -1.94, -2.5$. The predicted

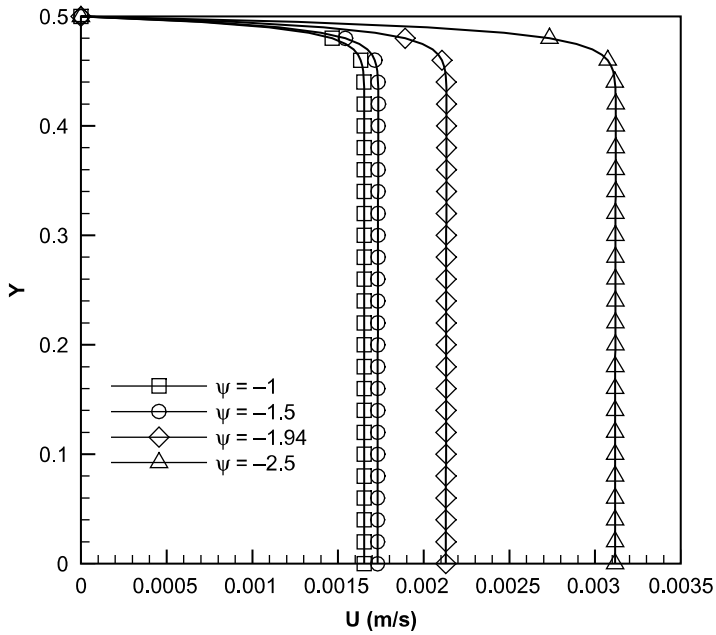

Figure 9.
Comparison of the predicted velocity profiles u (2.5, y) for the cases investigated at two different values of $\psi = -1, -1.5, -1.94, -2.5$

temperature profiles for $T(x, 0)$ and $T(0.5, y)$ have been compared and plotted in Figures 10 and 11. With the increased wall zeta potential, a smaller amount of Joule heat will be generated and can be added to the fluid. This explains the reason for the temperature $T(x, 0)$ plotted in Figure 10. For completeness, we also compare the profiles of ψ against y in Figure 12 at different wall zeta potentials. According to Figure 9, which plots u (2.5, y), one can clearly see that the predicted u-velocity slope (or $\partial u/\partial y$) for the case with $\psi_{wall} = -1.94$ is sharper than that investigated at $\psi_{wall} = -1$. This implies that the boundary layer shown in Figure 13 is thinner for the case with $\psi_{wall} = -1.94$.

Due to charge separation in the transverse direction, one can observe the EDL that contains the immobile ions near the Stern layer and the thermally induced mobile ions in its surrounding diffuse layer. The Debye length which characterizes the thickness of diffuse layer λ_D is inversely proportional to the square of ionic strength $\mathbf{I}$ and is proportional to the square of electrolyte temperature T, implying that $\lambda_D \sim \sqrt{T/\mathbf{I}}$. For this reason, we plot the distribution of $T^{1/2}(x)$ along $y = 0.5$ in Figure 14 to enlighten how the Debye length is varied along the streamwise direction.

Since the pressure and electrokinetic forces are dominant in their respective regions, we plot their ratio in Figure 15. It can be clearly seen from the computed ratio that the electrokinetic force plays a more important role in the diffuse layer. Apart from the wall, the electrokinetic force is decreased rapidly to zero. For the sake of clarity, we plot in Figure 16 the edges of Stern layer, Debye length, and the velocity boundary layer based on the simulation carried out in the domain with the grid size of 1/200.

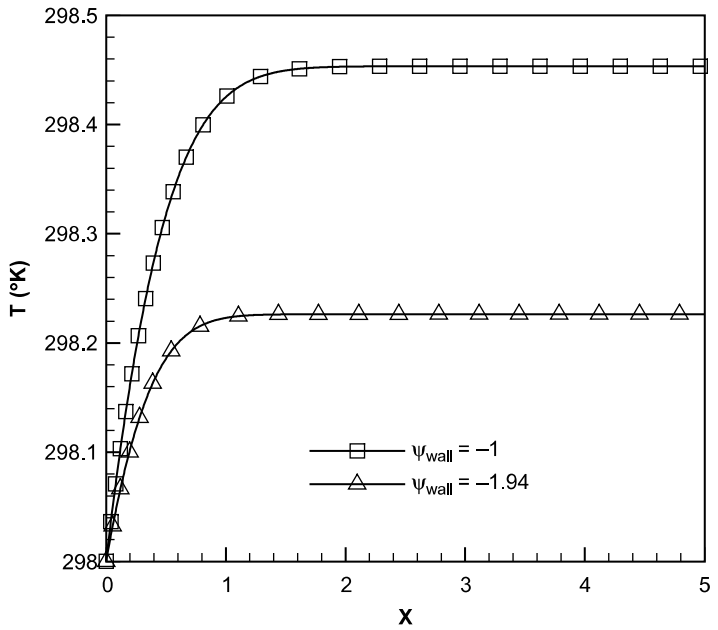

Figure 10.
The predicted temperature profiles $T(x, 0)$ for the cases investigated at the fixed electrical conductivity λ_1

Notes: (a) $\psi = -1$; (b) $\psi = -1.94$

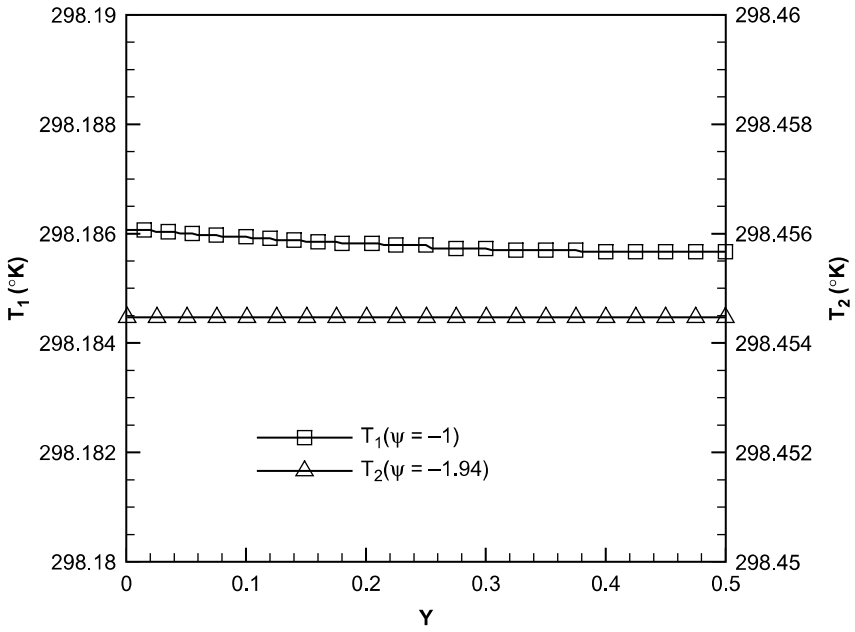

Notes: □for the temperature T_1 computed at $\psi = -1$ and Δ for the temperature T_2 computed at $\psi = -1.94$

Figure 11.
The predicted temperature profiles T (0.5, y) for the cases investigated at the fixed electrical conductivity λ_1

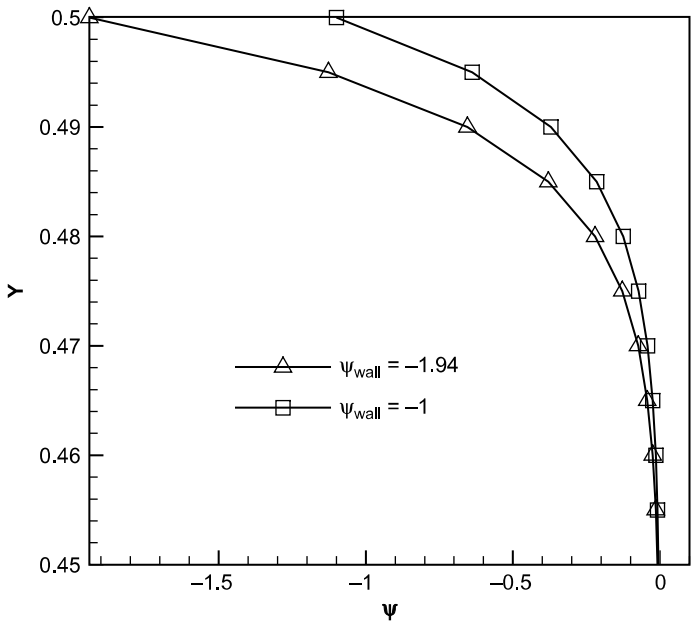

Figure 12.
Comparison of the predicted profiles for ψ against y at $x = 2.5$

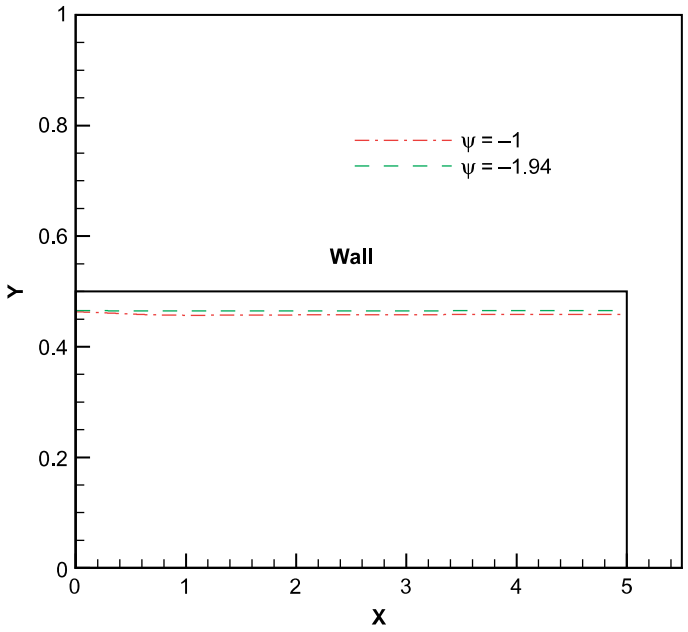

Figure 13.
Comparison of the velocity boundary layers for the cases investigated at $\psi_{wall} = -1.94$ and -1

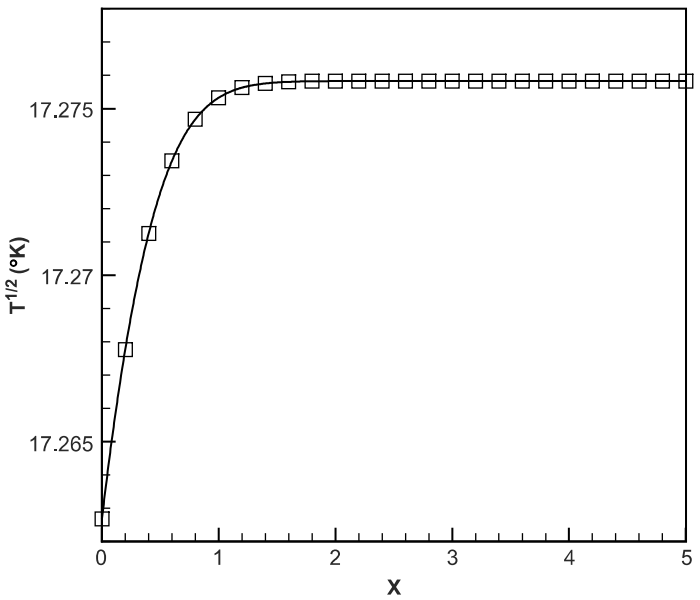

Figure 14.
Plot of the temperature $T^{1/2}$ against x at the plane of symmetry (at $y = 0$)

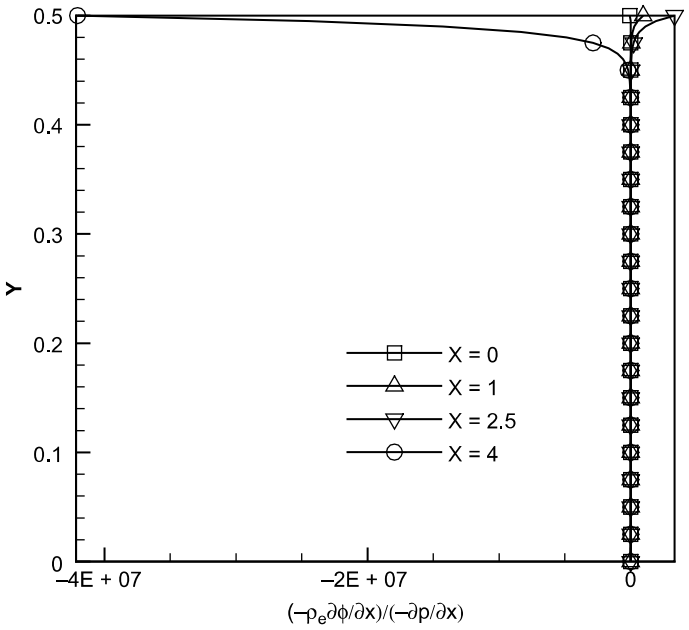

Figure 15.
The computed ratios of the electrokinetic and pressure gradient forces, which are plotted against y at $x = 3$

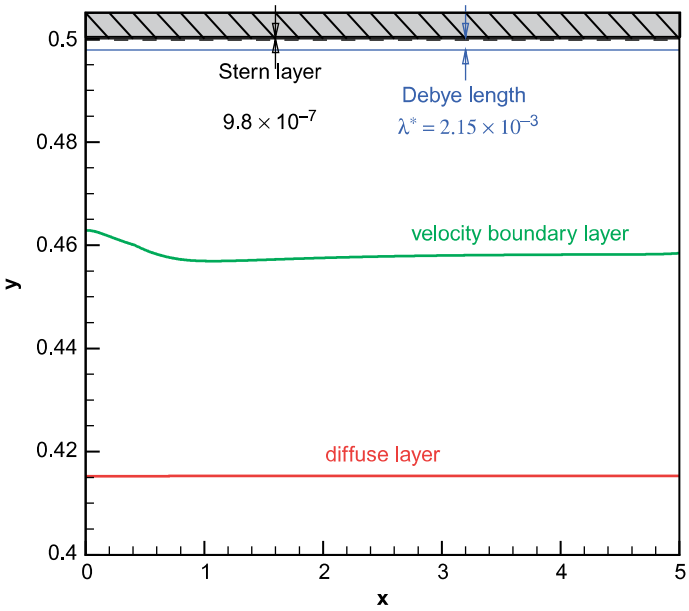

Figure 16.
The predicted edges of the diffuse layer, velocity boundary layer and Debye length

6. Concluding remarks

In this study the mixed electroosmotic/pressure-driven flow in the straight microchannel is studied with the emphasis on the Joule heat in the equations of motion. The nonlinear behaviors resulting from the hydrodynamic, thermal and electrical three-field coupling and the temperature-dependent fluid viscosity, thermal conductivity, electrical permittivity, and conductivity of the investigated buffer solution are analyzed. In the non-staggered grids, the locally analytic one-dimensional CDR scheme is applied in the predictor-corrector two steps to predict the sharply varying field variables without rendering numerical oscillations. The solutions computed from the employed flux discretization scheme for the hydrodynamic, thermal and electric field equations have been verified to have good agreement with the analytical solution. Parametric studies have been carried out by varying the electrical conductivity at the fixed zeta potential and varying the zeta potential at the fixed electrical conductivity. Conclusions drawn from the computed solutions are as follows. Electrokinetic force, which was found to be dominant in the diffuse layer, is rapidly decreased to zero in the direction towards the channel core. A sharp velocity profile near the channel wall and the plateau-like velocity profile in the channel core are therefore developed. The maximum temperature along the streamwise direction was predicted at a location slightly downstream of the middle channel, followed by a monotonic decrease in the direction towards the channel exit. Since the region immediately adjacent to the channel wall plays a dominant role in determining the EOF phenomena, we have computed the edges of diffuse layer, velocity boundary layer, in addition to the calculation of Debye length, to reveal the electroosmotic flow structure.

References

Arnold, A.K., Nithiarasu, P. and Tucker, P.G. (2008), "Finite element modeling of electroosmotic flows using unstructured meshes", *J. of Numerical Methods for Heat and Fluid Flow*, Vol. 18, pp. 67-82.

Burgreen, D. and Nakache, F.R. (1964), "Electrokinetic flow in ultrafine capillary sites", *J. Physical Chemistry*, Vol. 68, pp. 1084-91.

Chakraborty, S. (2006), "Analytical solutions of Nusselt number for thermally fully developed flow in microtubes under a combined action of electroosmotic forces and imposed pressure gradients", *J. Heat and Mass Transfer*, Vol. 49, pp. 810-13.

Das, S. and Chakraborty, S. (2007), "Transverse electrodes for improved DNA hybridization in microchannels", *AIChE Journal*, Vol. 53 No. 5, pp. 1086-99.

Das, S., Das, T. and Chakraborty, S. (2006), "Modeling of coupled momentum, heat transfer and solute transport during DNA hybridization in a channel in the presence of electroosmotic effects and axial pressure gradients", *Microfluid Nanofluid*, Vol. 2, pp. 37-49.

Dutta, P. and Breskok, A. (2001), "Analytical solution of combined electroosmotic/pressure driven flows in two-dimensional straight channels: finite Debye layer effects", *Anal. Chem.*, Vol. 73, pp. 1979-86.

Garai, A. and Chakraborty, S. (2009), "Micro scale thermo-fluidic transport in two incompressible liquid layers subject to combined electroosmotic and pressure-driven transport", *J. of Heat and Mass Transfer*, Vol. 52, pp. 2660-6.

Horiuchi, K. and Dutta, P. (2004), "Joule heating effects in electroosmotically driven microchannel flows", *Int. J. Heat and Mass Transfer*, Vol. 47, pp. 3085-95.

Hunter, R.J. (1981), *Zeta Potential in Colloid Science Principles and Applications*, Academic Press, New York, NY.

Lin, H., Storey, B.D., Oddy, M.H., Chen, C.H. and Santiago, J.G. (2004), "Instability of electrokinetic microchannel flows with conductivity gradients", *Physics of Fluids*, Vol. 16, pp. 1922-35.

Masliyah, J.H. (1994), *Electrokinetic Transport Phenomena*, Alberta Oil Sands Technology and Research Authority, Edmonton.

Nithiarasu, P. and Lewis, R.W. (2008), "A short note on Joule heating in electro-osmotic flow: a consistent non-dimensional scaling", *J. of Numerical Methods in Heat and Fluid Flow*, Vol. 18, pp. 919-31.

Patankar, S.V. (1980), *Numerical Heat Transfer and Fluid Flow*, Hemisphere, New York, NY.

Peaceman, D.W. and Rachford, H.H. (1955), "The numerical solution of parabolic and elliptic differential equations", *J. Soc. Ind. Appl. Math.*, Vol. 3, pp. 28-41.

Probstein, R.F. (1994), *Physicochemical Hydrodynamics: An Introduction*, 2nd ed., Wiley, New York, NY.

Reuss, F.F. (1809), "Charge-induced flow", *Proceedings of the Imperial Society of Naturalists Moscow*, Vol. 3, pp. 327-44.

Sheu, Tony W.H. and Chiu, P.H. (2007), "A divergence-free-condition compensated method for incompressible Navier-Stokes equations", *Computer Methods in Applied Mechanics and Engineering*, Vol. 196, pp. 4479-94.

Sheu, Tony W.H. and Lin, R.K. (2003), "An incompressible Navier-Stokes model implemented on non-staggered grids", *Numer. Heat Transf., B Fundam.*, Vol. 44 No. 3, pp. 277-94.

Sheu, Tony W.H., Sheu, S.K. and Wang, R.K. (2000), "An implicit scheme for solving the convection-diffusion-reaction equation in two dimensions", *J. Comput. Phys.*, Vol. 164, pp. 123-42.

Singh, S.P., Nithiarasu, P., Eng, P.F., Lewis, R.W. and Arnold, A.K. (2008), "An implicit-explicit solution method for coupled electroosmotic flows in three dimensions using the unstructured meshes", *Int. J. for Numerical Methods in Engineering*, Vol. 73, pp. 1137-52.

Storey, B.D. (2005), "Direct numerical simulation of electrohydrodynamic flow instabilities in microchannels", *Physica D*, Vol. 211, pp. 151-67.

Tang, G.Y., Yang, C., Chai, C.J. and Gong, H.Q. (2003), "Modeling of electroosmotic flow and capillary electrophoresis with the Joule heating effect: the Nernst-Planck equation versus the Boltzmann distribution", *Langmuir*, Vol. 19, pp. 10975-84.

Tang, G.Y., Yang, C., Chai, C.J. and Gong, H.Q. (2004), "Joule heating effect on electroosmotic flow and mass species transport in a microcapillary", *Int. J. Heat and Mass Transfer*, Vol. 47, pp. 215-27.

Tang, G.Y., Yan, D., Yang, C., Gong, H.Q., Chai, C.J. and Lam, Y.C. (2006), "Assessment of Joule heating and its effects on electroosmotic flow and electrophoresis transport of solutes in microfluidic channels", *Electrophoresis*, Vol. 27, pp. 628-39.

Weast, R., Astle, M.J. and Beyer, W.H. (1986), *CRC Handbook of Chemistry and Physics*, CRC Press, Boca Raton, FL.

Corresponding author
Tony W.H. Sheu can be contacted at: twhsheu@ntu.edu.tw